Hindawi Publishing Corporation
Journal of Nanomaterials
Volume 2016, Article ID 3170142, 9 pages
http://dx.doi.org/10.1155/2016/3170142

Research Article

Spark Plasma Sintered Si_3N_4/TiN Nanocomposites Obtained by a Colloidal Processing Route

L. A. Díaz,[1,2] W. Solís,[2] P. Peretyagin,[2] A. Fernández,[1] M. Morales,[3] C. Pecharromán,[3] J. S. Moya,[1,2] and R. Torrecillas[1,2]

[1]*Multifunctional Nanomaterials and Nanocomposites, Centro de Investigación en Nanomateriales y Nanotecnología (CINN), Consejo Superior de Investigaciones Científicas, Universidad de Oviedo, Principado de Asturias, Avenida de la Vega 4-6, El Entrego, 33940 Asturias, Spain*
[2]*Laboratory of Electric Currents and Sintering Technologies (LECAST), Moscow State University of Technology (STANKIN), Vadkovskiy Pereulok 1, Moscow 127994, Russia*
[3]*Group of Bioinspired Materials, Instituto de Ciencia de Materiales de Madrid (ICMM), Consejo Superior de Investigaciones Científicas (CSIC), C/Sor Juana Inés de la Cruz 3, Cantoblanco, 28049 Madrid, Spain*

Correspondence should be addressed to L. A. Díaz; la.diaz@cinn.es

Received 9 December 2015; Revised 3 February 2016; Accepted 14 February 2016

Academic Editor: Claude Estournès

Ceramic Si_3N_4/TiN (22 vol%) nanocomposites have been obtained by Spark Plasma Sintering (SPS). Our colloidal processing route allows obtaining dispersed nanoparticles of TiN smaller than 50 nm avoiding the presence of agglomerates. The nanostructured starting powders were obtained by using a colloidal method where commercial Si_3N_4 submicrometer particles were coated with anatase TiO_2 nanocrystals. A later nitridation process led to the formation of TiN nanoparticles on the surface of Si_3N_4. A second set of powders was prepared by doping the above defined powders with yttrium and aluminium precursors using also a colloidal method as sources of alumina and yttria. After thermal nitridation and SPS treatment, it has been found that the addition of oxides dopants improves the mechanical performance (K_{IC}, σ_f) but increases the electrical resistivity and significantly reduces the hardness. This is due to the formation of a continuous insulating glassy phase that totally envelops the conductive TiN nanoparticles, avoiding the percolative contact between them. The combination of colloidal processing route and SPS allows the designing of tailor-made free glassy phase Si_3N_4/TiN nanocomposites with controlled microstructure. The microstructural features and the thermoelectrical and mechanical properties of both kinds of dense SPSed compacts are discussed in this work.

1. Introduction

Silicon nitride is among the most important ceramic materials for high-temperature applications because of its combination of mechanical properties at room and high temperatures, oxidation resistance, low coefficient of thermal expansion, and low density in comparison to refractory metals [1]. In 1991, Niihara [2] introduced the ceramic nanocomposite concept and demonstrated that silicon nitride matrix composites containing dispersed nanosized SiC particles exhibit enhanced high-temperature strength and creep resistance when compared with monolithic silicon nitride. The addition of TiN to ceramic matrix composites has been widely studied. Improvement of mechanical properties as well as a reduction of the electrical resistivity of the compacts has been reported, making electrodischarge machining of the resulting dense composites possible [3–6].

High performance silicon nitride materials were developed for automotive engine wear parts and also as cutting tools. In this case, the introduction of titanium nitride (TiN), with a high melting temperature (>3000°C), good electrical conductivity, and high resistance to corrosion and oxidation, improves the wear resistance in continuous cutting tools [7]. On the other hand, this conductive ceramic has been recently revealed as a possible substitute of plasmonic metals, because of its lower cost, and it is possible to modify the electron density by doping. In this sense, new functional

applications can be developed in visible and near-infrared optics by depositing dispersed nanometer size TiN particles on transparent matrices [8]. Strictly focusing on the mechanical properties of dense ceramics, the difficulty of machining typical monolithic silicon nitride blocks (electrical resistivity $> 10^{11}\ \Omega$·cm) into complex shapes because of their high toughness and hardness makes the introduction of TiN nanoparticles a simple and efficient way to transform silicon nitride materials electrodischarge machining compatible. The standard procedure to obtain TiN-Si_3N_4 composites is usually based on sintering of mechanically mixed powders, but this method does not allow homogeneous dispersion of TiN nanoparticles into the Si_3N_4 matrix. Alternatively, the colloidal route has already demonstrated its potential to process ceramic oxides and/or nonoxide/oxide mixtures [9–14]. It is important to distinguish that among colloidal processing routes there are included processes based only on wet mixing of nanopowders and processes in which the nucleation of a second phase onto the surface of starting powders working with precursors in solution is promoted. This second route is what is employed in this work. Concerning sintering process, during the last years, Spark Plasma Sintering (SPS) has emerged as a very promising technology for these materials [15–21]. This technique allows obtaining high density materials in short processing times leading to microstructure control unattainable by other technologies. It must be taken into account that microstructural design is limited by the average grain size of starting powders and the sintering conditions, which are responsible for the grain growth during densification. In this work, for the first time, the preparation of TiN-Si_3N_4 composites combining a colloidal processing route for preparing nanocomposite starting powders and Spark Plasma Sintering as consolidation technique is studied. The colloidal processing method has been revealed to be flexible enough to include multiple phases or doping, which have a dramatic effect on the physical properties of the final nanocomposite. The incorporation of sintering additives is explored and resulting materials are characterized in terms of mechanical and thermoelectrical properties.

2. Experimental Procedure

Undoped α-Si_3N_4 powders ($\alpha > 95\%$) (Hubei Minmetals, China) with a mean particle size of 0.5 μm were used as starting material. In Figure 1, the flow charts of the processing routes followed for preparing the different nanocomposite powders are shown. Figure 1(a) shows a flow chart corresponding to the doping of the starting α-Si_3N_4 with 3 wt% of Al_2O_3 and 5 wt% of Y_2O_3. A stable suspension in anhydrous ethanol (99.70%) (Panreac, Spain) of α-Si_3N_4 powders was doped by dropwise addition of a diluted yttrium ethoxide ($C_9H_{21}O_6Y$) (ABCR, Germany) solution and a second aluminium chloride ($AlCl_3$) (ABCR, Germany) solution where the following reaction took place to form the corresponding aluminium ethoxide: $AlCl_3 + 3EtOH = Al(OEt)_3 + 3HCl$ [22, 23]. After magnetic stirring at 60°C and drying at 120°C for 24 h in order to eliminate any traces of alcohol, the powders were sieved under 63 μm and thermally treated at 850°C for 2 h in order to remove organic residuals and form amorphous Al_2O_3 and Y_2O_3 particles on the surface of the α-Si_3N_4 particles. These powders are labelled as AY-Si_3N_4 powders.

Figure 1(b) shows a flow chart corresponding to the synthesis of nano-TiN-coated Si_3N_4 particles. As starting materials, undoped Si_3N_4 and AY-Si_3N_4 powders, titanium isopropoxide ($C_{12}H_{28}O_4Ti$) (ABCR, Germany), and absolute ethanol (99.70% purity) (Panreac, Spain) were used. By this way, undoped Si_3N_4 and AY-Si_3N_4 powders with addition of 22 vol% TiN nanoparticles were prepared following the colloidal processing route developed by Schehl et al. [9]. A stable suspension of silicon nitride powders in absolute ethanol was doped by dropwise addition of a diluted titanium alkoxide solution. After magnetic stirring at 60°C and drying at 120°C for 24 h in order to eliminate any traces of alcohol, the powders were sieved under 63 μm and thermally treated at 500°C for 2 h, removing organic residuals and forming TiO_2 nanoparticles. Then, the powders were subjected to nitridation by flowing NH_3 gas (250 mL/min) at 1000°C for 3 h. Powders were labelled as Si_3N_4/TiN and AY-Si_3N_4/TiN, respectively, depending on the starting silicon nitride powder used.

Thermal evolution of the precursor-coated powders was analyzed by DSC/TGA (TA Instruments, model 2960) and the crystalline phases were identified by XRD (Bruker, D-5000) for both sets of doped and undoped Si_3N_4 powders.

The size and shape of the TiO_2 and TiN particles were determined by TEM observation (JEOL, 2000 EX II). Finally, the powders were attrition milled for 1 h in order to break agglomerates, dried, and sieved under 63 μm. These powders were introduced in graphite moulds (40 mm diameter) and subjected to different SPS treatments in FCT System GmbH (Germany) model HPD-25, at 1800°C for 2 min and applying a maximum pressure of 100 MPa at 1100°C, with a heating rate of 100°C/min up to 600°C and then of 110°C/min up to the final sintering temperature. The density of the sintered materials was determined by using Archimedes' method in water at room temperature. The theoretical density of the different materials was calculated by using the law of mixtures equation taking as theoretical densities 5.43 g/cm^3 and 3.19 g/cm^3 for TiN and Si_3N_4, respectively. Microstructural characterization of polished and etched surfaces, using CF_4 gas (plasma system type Femto, Diener Electronic, Germany), was carried out with a field emission scanning electron microscope (FESEM FEI: Quanta FEG 650), with associated Energy Dispersive Spectroscopy (EDS) equipment from EDAX-AMETEK GmbH (Germany). In the present work, the evaluation of average grain size of polycrystalline ceramics was obtained by the lineal intercept technique, which involves measurements taken from polished sections [24].

Four-point flexural strength of six bars with $3 \times 4 \times 35$ mm dimensions (10–21 mm span) was determined by using an Instron machine model 8562, according to the ASTM F 394-78 standard. The fracture toughness measurements (K_{IC}) were performed using the single-edge-notched-beam (SENB) technique ($a/w = 0.4$ and notch radius $\approx 100\ \mu$m), following

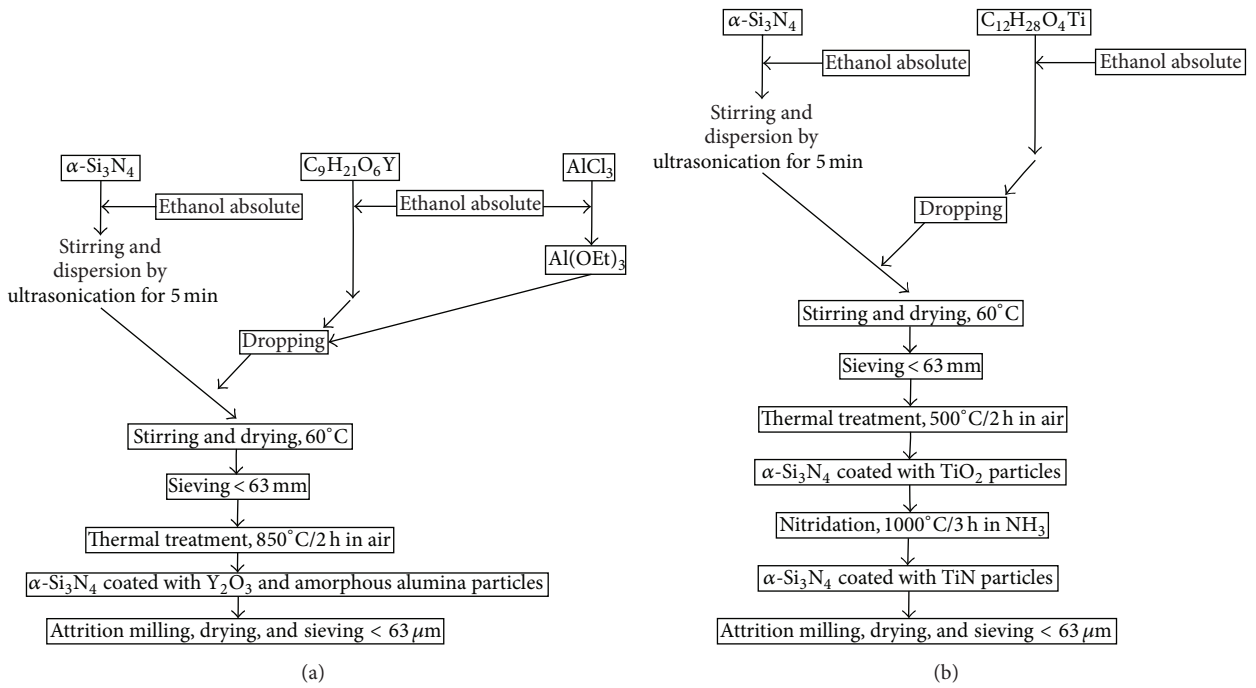

Figure 1: Flow chart corresponding to the doping of the α-Si_3N_4 starting powders with aluminium, yttrium, and titanium precursors.

the guidelines described in the ASTM C1421 standard. Vickers hardness was measured by using a durometer Micrometer 5103 (Buehler), loading 300 g for 10 seconds and making 30 measurements for sample.

Thermal conductivity measurements were made using the laser flash LFA 457 Microflash equipment (NETZSCH, Germany). Experiments were done in nitrogen atmosphere at 25, 300, 600, and 900°C, attending the ASTM E-1461 and DIN EN 821 norms. The experimental data were analyzed by the Cape-Lehman model and "Pulse Correction" both implemented in the equipment software. The specific heat (C_p) as a function of temperature was calculated using DSC equipment TA Instruments, model 2960.

The electrical resistivity of the samples was measured by different procedure depending on their conductivity. For the highly conductive samples, the four-point technique was employed, using a Keithley 6220 precision current source and Keithley 2182A nanovoltmeter. Conductivity data were obtained by the "Haldor Topsoe" correction [25]. In the case of highly resistive samples, silver paste electrodes were painted on the surfaces of thin pieces (thickness ~ 0.6 mm). For static values, a Keithley 6517A electrometer was employed, complemented in the case of high voltage ($V > 1$ kV) measurements by Heinzinger LNC10000 voltage source. Conductivity versus temperature ($T = 276$ to 386 K) measurements were performed by using a Peltier cell in N_2 atmosphere.

3. Results and Discussion

3.1. Characterization of Nanostructured Powders. In Figure 2, the thermogravimetric curves of the precursor-coated powders are shown. In both cases, it can be seen that the evolution of weight loss during heating is similar. Firstly, there are important weight losses at low temperatures (below 100–150°C) that correspond to the solvent that is retained on powder surface. Then, there is a continuous weight loss in which it is possible to distinguish changes in the curves slope. These changes can be rationalized considering the removal of the different organic compounds from the precursors used. However, in all cases, after 500°C, no more weight loss is observed and apparently all organic groups have been eliminated. The X-ray diffraction patterns of the samples are shown in Figure 3. The results showed that, after calcination at 850°C/2 h of AY-Si_3N_4 powders, amorphous alumina-yttria coated Si_3N_4 powders (Figure 3(a)) are obtained. In the case of powders doped with Ti precursor, the titanium oxide coating formed on silicon nitride particles after thermal treatment is anatase (Figure 3(b_1)) and transforms to TiN after nitridation by NH_3 gas (Figure 3(b_2)).

Figure 4 shows the TEM micrographs of the different synthesized powders. From these photomicrographs, it is possible to observe the homogeneous surface distribution of TiO_2 nanoparticles with a crystal size ranging from 3 to 20 nm that have been nucleated on the surface of Si_3N_4 particles (Figure 4(a)). After nitridation, the crystal size of TiN nanoparticles is smaller than 50 nm (Figure 4(b)). Then, the grain size of TiN nanoparticles is directly related to the grain size of the synthesized anatase nanoparticles. Figure 4(c) shows the homogeneous coating of Si_3N_4 powders with alumina and yttria after calcination steps and Figure 4(d) shows how this homogeneous coating is maintained after the nucleation of TiN nanoparticles. These results clearly indicate that the colloidal processing route is a fully effective process for nucleating nanoparticles directly attached to the Si_3N_4 particles surface.

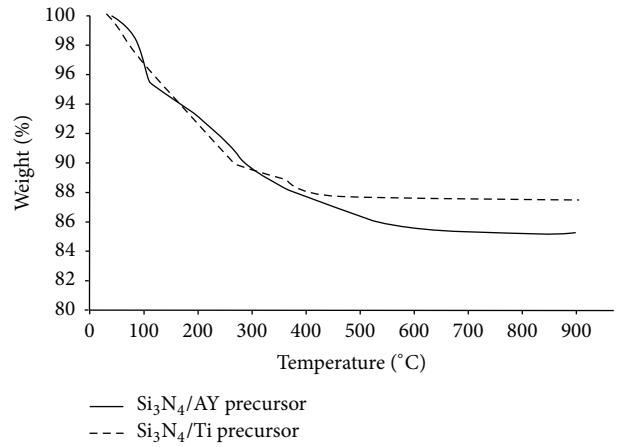

Figure 2: Thermogravimetric curves of the precursor-coated powders (continuous line: Si_3N_4 coated with alumina and yttria precursors; dashed line: Si_3N_4 coated with titanium precursor).

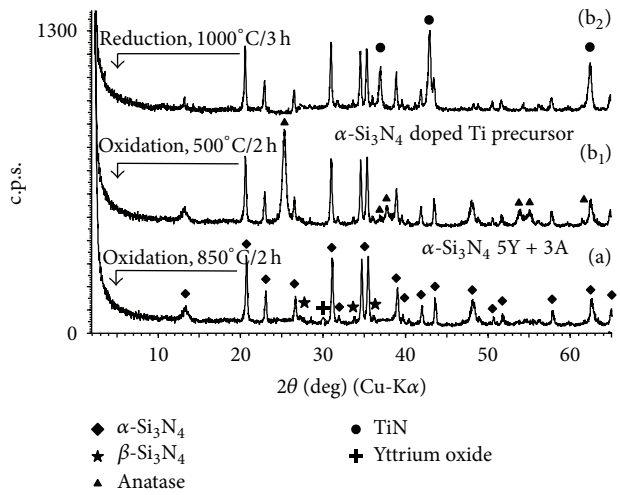

Figure 3: XRD analysis of doped powders after thermal treatments. (a) α-Si_3N_4 starting powders doped with Al and Y precursors and thermally treated at 850°C/2 h. (b_1) α-Si_3N_4 starting powders doped with Ti precursor and oxidized at 500°C/2 h. (b_2) The same powders are subjected to a thermal treatment reduction with NH_3 gas at 1000°C/3 h.

3.2. Characterization of Dense Nanocomposites. Figure 5 shows the evolution of the material density as a function of the sintering temperature for the case of Si_3N_4/TiN SPSed samples. From this data, it can be stated that full density is only achieved for a final sintering temperature of 1800°C. Figure 6 shows the microstructure of the composites sintered and the corresponding XRD patterns. FESEM photomicrograph of the SPSed composites obtained at 1800°C/100 MPa/2 min using the Si_3N_4/TiN powders is shown in Figure 6(a). The compact is very homogeneous showing two equiaxial phases: (i) the white one corresponds to TiN (200 nm, ±90 nm) and (ii) the grey one corresponds to α-Si_3N_4 (290 nm, ±150 nm). No glassy phase was detected by FESEM. In Figure 6(b), we can also observe FESEM photomicrograph of AY-Si_3N_4/TiN SPS sintered under the same conditions, 1800°C/100 Mpa/2 min. In this case, the presence of both equiaxial α-Si_3N_4 (315 nm, ±120 nm) and elongated β-Si_3N_4, (300 nm, ±120 nm) as well as the TiN phase (700 nm, ±130 nm) is shown. In this photomicrograph, we can clearly observe the presence of a continuous glassy phase wetting both phases as it has been classically observed in other alumina and yttria doped Si_3N_4 materials [26–28]. Figure 6(c) shows the FESEM photomicrograph corresponding to AY-Si_3N_4/TiN sintered for a longer stay time (1800°C/100 Mpa/2 min). The presence of β-Si_3N_4 (430 nm, ±120 nm), TiN crystals (930 nm, ±130 nm), and sinoite (Si_2N_2O) can be observed, with the α-Si_3N_4 phase undetected. Appearance of Si_2N_2O phase (sinoite) is related to the oxidation layer of α-Si_3N_4 inherent of the starting particles (detected by XPS and not shown). The carbothermal reduction of SiO_2 occurred according to the following reaction:

$$2SiO \longrightarrow Si + SiO_2 \quad (1)$$

Subsequently, the following reaction occurs:

$$3Si + SiO_2 + 2N_2 \longrightarrow 2Si_2N_2O \quad (2)$$

which involves vapor phases of SiO and N_2 and gives Si_2N_2O phase. Then, increasing the stay time at high temperature promotes the notion that side reactions occur leading to the formation of third phases.

The electrical resistivity of the materials gives valuable information about the microstructure of the composites. In the case of the oxide-free phase, the oxide-free sample, α-Si_3N_4-22 vol% TiN, was revealed to be an excellent conductor with resistivity as low as 1.8×10^{-3} Ω·cm, well below 100 Ω·cm, the maximum allowed value to be machined by electrodischarge machining (EDM) [29, 30]. It should be recalled that pure α-Si_3N_4 phase is a relatively good insulator with DC resistivity around 10^{11} Ω·cm [31, 32]. In this sense, the inclusion of TiN nanoparticles raised the conductivity by 14 orders of magnitude. This is a remarkable result and is mostly due to the excellent degree of dispersion of TiN nanoparticles around α-Si_3N_4 crystals, a result which is especially difficult when using conventional mixing methods with nanosize TiN powders.

However, such low values of resistivity disappear when the nanostructured particles are sintered in the presence of alumina and yttria. In this regard, in Figure 7(a), conductivity of these materials as a function of both electric field and temperature appears. The resistivity at room temperature and low electric field resulted to be of the order of $\rho \sim 10^{13}$ Ω·cm. This value, which is even higher than the monolithic α-Si_3N_4, suggests that there is an insulating glassy phase covering totally the conductive TiN nanoparticles avoiding the percolative contacts between them. In this regard, it has been found that conductivity follows Schottky mechanism from the variation of the current density versus the applied field (data not shown). This result suggests that conductive nanostructured microparticles are completely embedded by an insulating phase. By measuring the current density versus temperature, it is easy to determine the barrier potential height. In Figure 7(b), the Arrhenius plots determine that

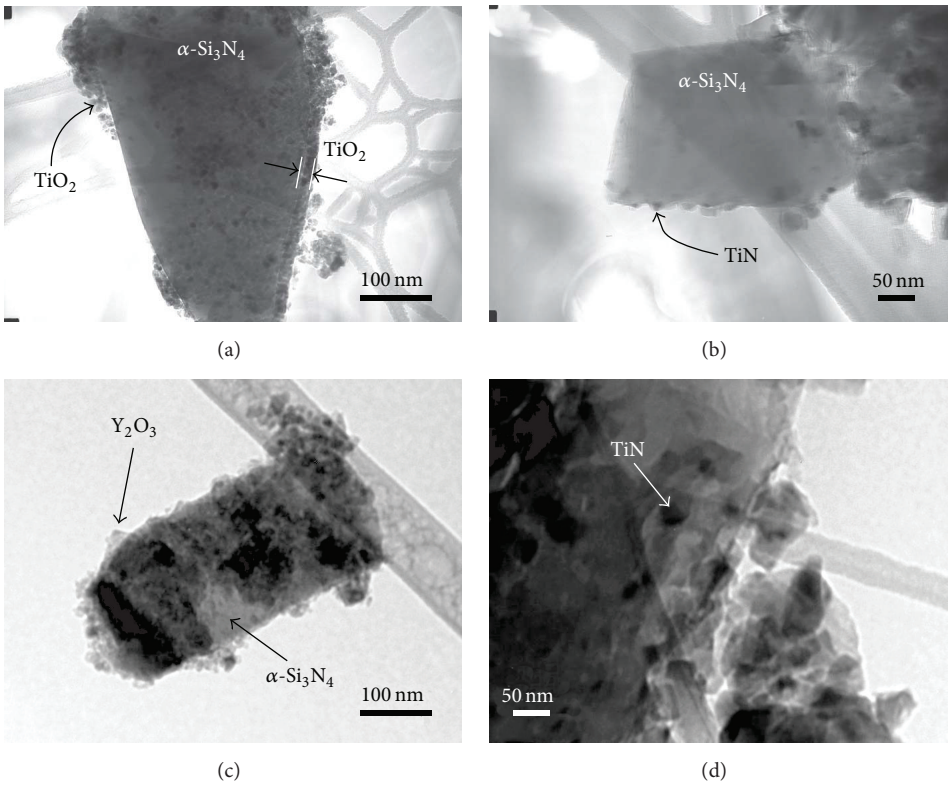

Figure 4: TEM images of the different nanostructured starting powders prepared: (a) Si_3N_4/TiO_2, (b) Si_3N_4/TiN, (c) AY-Si_3N_4/TiO_2, and (d) AY-Si_3N_4/TiN.

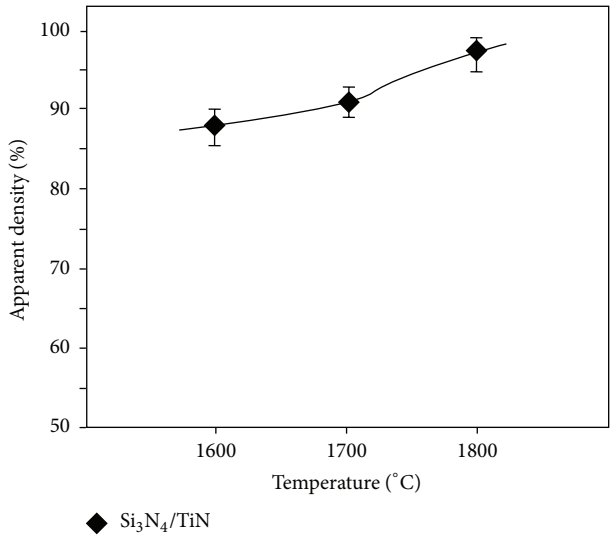

Figure 5: Apparent density results versus temperature for the case of Si_3N_4/TiN SPSed compacts.

for samples AY-Si_3N_4/TiN dwell 2 min and AY-Si_3N_4/TiN dwell 10 min the activation energies are quite low (dwell 2 min E_a = 0.18 eV and dwell 10 min E_a = 0.16 eV) suggesting that conductive grains could be embedded by a thin grain boundary made by multicomponent silica glass. The effect of transition metals as Ti and Y on silica based glass could introduce localized states into the band gap of silica glass, notably lowering the conductivity activation energy. However, this phase is quite scarce, due to the low value of the resulting low temperature resistivity. These results are in excellent agreement with the thermal conductivity versus temperature measurements of the studied samples (Figure 8). As it is clearly observed, the presence of glassy phase in the AY-Si_3N_4/TiN samples notably increased the thermal conductivity values in the room temperature to 900°C range. Also, in these samples, thermal conductivity could further be improved through increasing the β/α Si_3N_4 phase ratio during nitridation and enhancing grain growth during SPS sintering [33].

Table 1 shows the main mechanical properties of both types of composites. Hardness of free glassy phase nanocomposites was found to be around 20 GPa whereas in the doped sample this value decreases down to 16 GPa. This fact can be rationalized considering the smaller grain size value of pure Si_3N_4-TiN composite and the absence of a continuous glassy phase. The presence of glassy phase is responsible for hardness decrease and simultaneously promotes significant increases in bending flexural strength and fracture toughness; in the case of doped materials, because of the occurrence of the glassy phase, α-Si_3N_4 to β-Si_3N_4 transformation takes place with classical elongated grains that have as a consequence the activation of the well-known reinforcement mechanisms by crack bridging/pull-out and/or crack deflection [34, 35] and consequently the increase of K_{IC} and σ_f

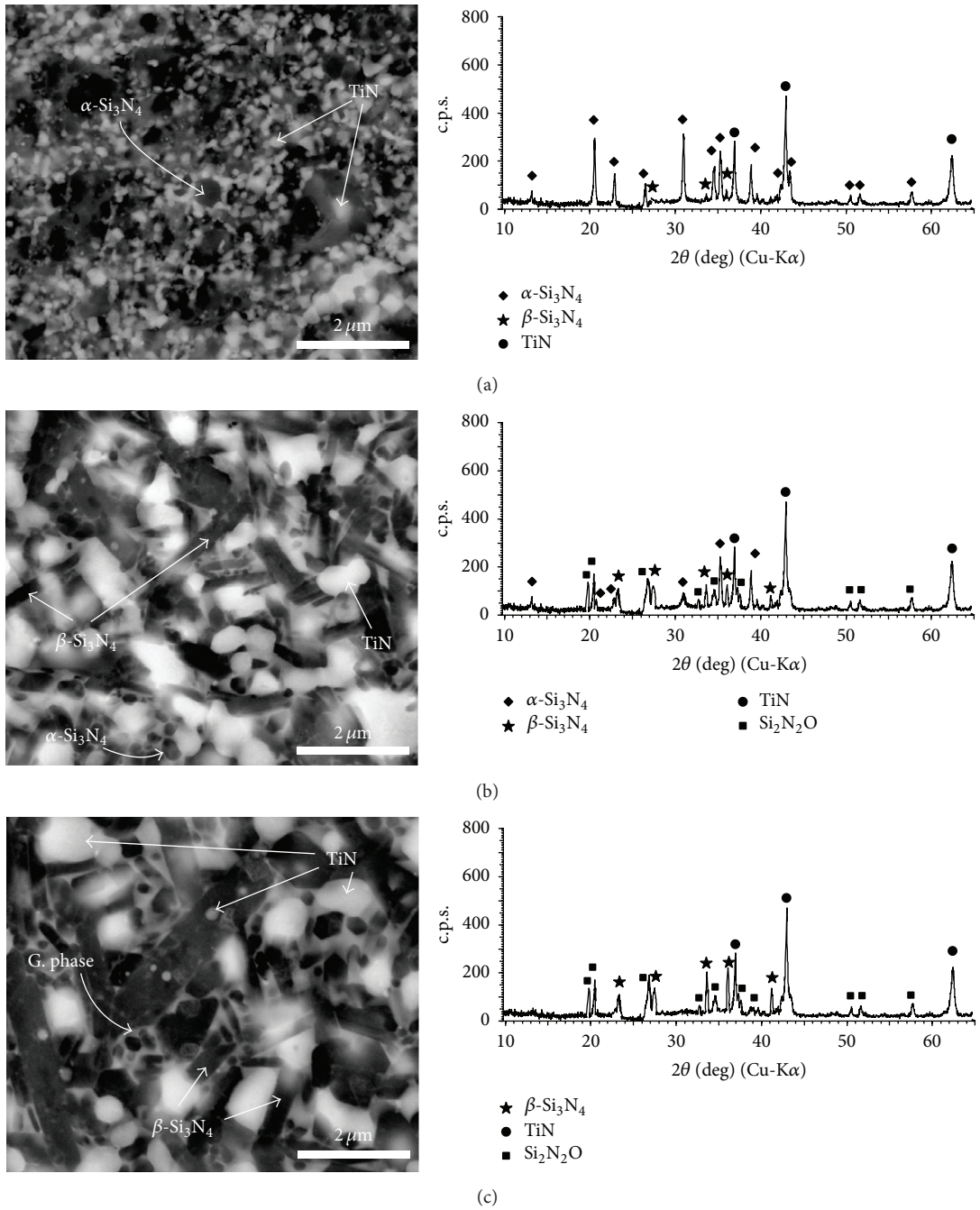

Figure 6: Microstructures by FESEM of dense Si_3N_4-TiN composites sintered at 1800°C and 100 MPa and the corresponding XRD patterns. (a) Si_3N_4/TiN dwell 2 min sample, (b) AY-Si_3N_4/TiN dwell 2 min sample, and (c) AY-Si_3N_4/TiN dwell 10 min sample (G. phase: glassy phase).

Table 1: Density and mechanical properties of sintered nanocomposites at 1800°C/100 MPa.

Sample	Density (g/cm^3)	Hardness (GPa)	Flexural strength (MPa)	Fracture toughness ($MPam^{1/2}$)
Si_3N_4-TiN 1800°C/100 MPa/2 min	3.58	19.7 ± 0.8	415 ± 34	2.5 ± 0.3
AY-Si_3N_4-TiN 1800°C/100 MPa/2 min	3.59	17.2 ± 0.8	519 ± 25	4.7 ± 0.3
AY-Si_3N_4-TiN 1800°C/100 MPa/10 min	3.56	15.8 ± 0.9	623 ± 18	5.5 ± 0.4

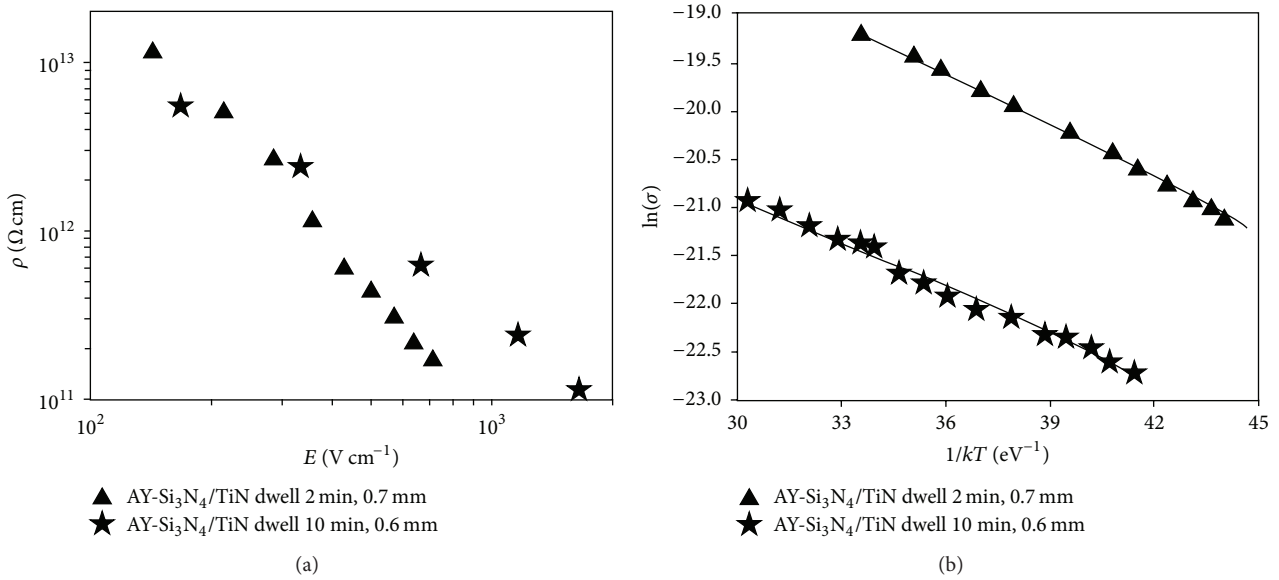

Figure 7: Evolution of electrical properties of AY-Si_3N_4/TiN composites. (a) Conductivity as a function of electric field and (b) current density as a function of maximum temperature.

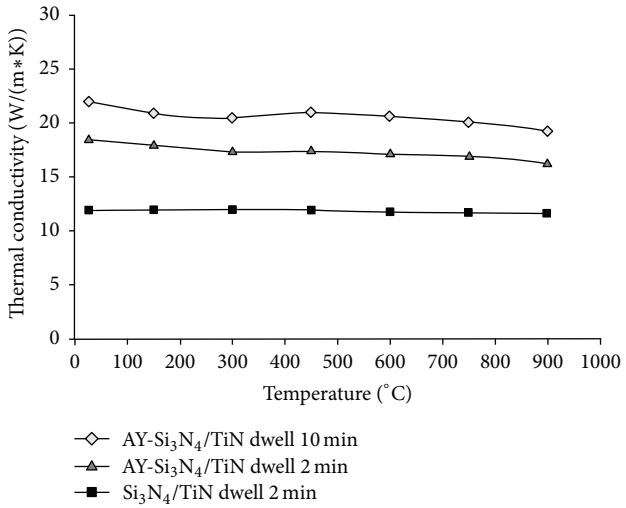

Figure 8: Thermal conductivity versus temperature of the composites sintered at 1800°C and 100 MPa.

values. $\alpha:\beta$ Si_3N_4 phase ratio was calculated from the peak heights of $\alpha(200)$ and $\beta(200)$ reflections [26]. According to sintering conditions (1800°C), the results showed that the undoped Si_3N_4/TiN composite has $\alpha:\beta = 3.56$ while AY-Si_3N_4/TiN samples have $\alpha:\beta = 0.29$ (dwell time 2 min).

The materials obtained without AY dopants have a lower mechanical performance (K_{IC} and σ_f values decrease); however, because of the finer microstructure, they present high hardness and on the top of this, this material presents an excellent electrical conductivity value allowing the use of machining technologies as EDM and even can be used at high temperatures thanks to the absence of glassy phase and in case where an extreme mechanical performance is not needed as, for instance, in bearings for high-temperature applications. Also, these materials can withstand more corrosive conditions than the classical Si_3N_4 materials thanks to the absence of the intergranular glassy phase.

4. Conclusions

Nano-TiO_2 (<10 nm) coated Si_3N_4 particles were fabricated following a simple colloidal processing route. The results were confirmed by XRD, FESEM, EDX, and TEM. The TiO_2 nanoparticles grew from 3 to 10 nm and after a nitridation process at 1000°C were converted to TiN nanoparticles of less than 25 nm attached to the Si_3N_4 crystals.

By using this powder, in the present work, it has been proven that, by SPS technique at 1800°C and 100 MPa, close to theoretical density nanocomposites free of intergranular glassy phase α-Si_3N_4-TiN (22 vol%) compacts with high hardness (20 GPa) and very low electrical resistivity (1.3×10^{-3} Ω·cm) can be fabricated. These dense SPSed samples can be EDM machined.

The addition of alumina and yttria as dopants improves the mechanical performance (K_{IC}, σ_f) but dramatically increases the electrical resistivity (1.3×10^{-3} Ω·cm versus ~ 10^{13} Ω·cm) and significantly reduces the hardness from 20 to 16 GPa. This is due to the formation of a continuous glassy phase that totally envelops the conductive TiN nanoparticles avoiding the percolative contact between them.

Combination of colloidal processing route and Spark Plasma Sintering technique allows the designing of tailor-made free glassy phase Si_3N_4/TiN nanocomposites with controlled microstructure. Due to the presence of well dispersed TiN nanoparticles (≤50 nm), this material can be used in new functional applications such as visible and near-infrared optics.

Conflict of Interests

The authors declare that there is no conflict of interests regarding the publication of this paper.

Acknowledgment

The authors would like to thank the Ministry of the Russian Federation that supported this work in the frame of Governmental Regulation of the Russian Federation no. 220, 9 April 2010, by Contract 14.B25.31.0012, June 26, 2013.

References

[1] M. Herrmann, H. Klemm, and C. Schubert, "Silicon nitride based hard materials," in *Handbook of Ceramic Hard Materials*, R. Riedel, Ed., vol. 2, pp. 749–801, Wiley-VCH, 2000.

[2] K. Niihara, "New design concept of structural ceramics—ceramic nanocomposites," *Journal of the Ceramic Society of Japan*, vol. 99, no. 1154, pp. 974–982, 1991.

[3] A. Bellosi, S. Guicciardi, and A. Tampieri, "Development and characterization of electroconductive Si_3N_4-TiN composites," *Journal of the European Ceramic Society*, vol. 9, no. 2, pp. 83–93, 1992.

[4] S. Kawano, K. Tsukurimichi, J. Takahashi, and S. Shimada, "Preparation of nano-sized TiN coated α-Si_3N_4 particles," *Journal of Materials Chemistry*, vol. 11, no. 10, pp. 2625–2628, 2001.

[5] S. Kawano, J. Takahashi, and S. Shimada, "Highly electroconductive TiN/Si_3N_4 composite ceramics fabricated by spark plasma sintering of Si_3N_4 particles with a nano-sized TiN coating," *Journal of Materials Chemistry*, vol. 12, no. 2, pp. 361–365, 2002.

[6] S. Kawano, J. Takahashi, and S. Shimada, "Fabrication of TiN/Si_3N_4 ceramics by spark plasma sintering of Si_3N_4 particles coated with nanosized TiN prepared by controlled hydrolysis of $Ti(O\text{-}i\text{-}C_3H_7)_4$," *Journal of the American Ceramic Society*, vol. 86, no. 4, pp. 701–705, 2003.

[7] M. Mitomo and Y. Tajima, "Sintering, properties and applications of silicon nitride and sialon ceramics," *Journal of the Ceramic Society of Japan*, vol. 99, no. 1154, pp. 1014–1025, 1991.

[8] U. Guler, V. M. Shalaev, and A. Boltasseva, "Nanoparticle plasmonics: going practical with transition metal nitrides," *Materials Today*, vol. 18, no. 4, pp. 227–237, 2015.

[9] M. Schehl, L. A. Díaz, and R. Torrecillas, "Alumina nanocomposites from powder-alkoxide mixtures," *Acta Materialia*, vol. 50, no. 5, pp. 1125–1139, 2002.

[10] M. Suárez, A. Fernández, J. L. Menéndez, J. Ramírez-Rico, and R. Torrecillas, "Blocking of grain reorientation in self-doped alumina materials," *Scripta Materialia*, vol. 64, no. 6, pp. 517–520, 2011.

[11] A. Borrell, V. G. Rocha, R. Torrecillas, and A. Fernández, "Surface coating on carbon nanofibers with alumina precursor by different synthesis routes," *Composites Science and Technology*, vol. 71, no. 1, pp. 18–22, 2011.

[12] I. Alvarez-Clemares, G. Mata-Osoro, A. Fernández et al., "Ceria doped alumina by Spark Plasma Sintering for optical applications," *Journal of the European Ceramic Society*, vol. 32, no. 11, pp. 2917–2924, 2012.

[13] J. A. Lewis, "Colloidal processing of ceramics," *Journal of the American Ceramic Society*, vol. 83, no. 10, pp. 2341–2359, 2000.

[14] M. Liu, L. Su, Y. Bi, H. Zhang, and Z. Fu, "Silicon nitride ceramic prepared by colloidal process," *Key Engineering Materials*, vol. 336–338, no. 3, pp. 2388–2390, 2007.

[15] D. S. Perera, M. Tokita, and S. Moricca, "Comparative study of fabrication of Si_3N_4/SiC composites by spark plasma sintering and hot isostatic pressing," *Journal of the European Ceramic Society*, vol. 18, no. 4, pp. 401–404, 1998.

[16] Z. Guo, G. Blugan, R. Kirchner, M. Reece, T. Graule, and J. Kuebler, "Microstructure and electrical properties of Si_3N_4-TiN composites sintered by hot pressing and spark plasma sintering," *Ceramics International*, vol. 33, no. 7, pp. 1223–1229, 2007.

[17] Z. Tatli, F. Çalişkan, J. Butler, C. Crowley, and S. Hampshire, "SPS sintering of silicon nitride with fluoride additive," *Ceramics International*, vol. 40, no. 1, part B, pp. 1399–1404, 2014.

[18] J. L. Huang and P. K. Nayak, "Microstructure evolution and mechanical properties of silicon nitride based ceramics sintered by spark plasma sintering (SPS)," in *Recent Advances in Ceramic Materials Research*, pp. 177–214, Nova Science, 2013.

[19] M. Zhou, D. Rodrigo, and Y.-B. Cheng, "Effects of the electric current on conductive Si_3N_4/TiN composites in spark plasma sintering," *Journal of Alloys and Compounds*, vol. 547, pp. 51–58, 2013.

[20] M. Zhou, J. Zhong, J. Zhao, D. Rodrigo, and Y.-B. Cheng, "Microstructures and properties of Si_3N_4/TiN composites sintered by hot pressing and spark plasma sintering," *Materials Research Bulletin*, vol. 48, no. 5, pp. 1927–1933, 2013.

[21] M. V. Zamula, A. V. Derevyanko, V. G. Kolesnichenko, O. B. Zgalat-Lozinskii, and A. V. Ragulya, "Production of products of various shapes from Si_3N_4-based refractory compounds by spark plasma sintering," *Powder Metallurgy and Metal Ceramics*, vol. 54, no. 1, pp. 8–15, 2015.

[22] W. H. Starnes Jr., S. Frantz, and H. T. Chung, "Aluminum chloride [alias its reaction product(s) with ethanol] for the stabilization of poly (vinyl chloride)?" *Polymer Degradation and Stability*, vol. 56, no. 1, pp. 103–108, 1997.

[23] L. A. Díaz, M. A. Montes-Morán, P. Y. Peretyagin et al., "Zirconia-alumina-nanodiamond composites with gemological properties," *Journal of Nanoparticle Research*, vol. 16, no. 2, article 2257, 2014.

[24] JC. Wurst and J. A. Nelson, "Lineal intercept technique for measuring grain size in two-phase polycrystalline ceramics," *Journal of the American Ceramic Society*, vol. 55, no. 2, pp. 109–111, 1972.

[25] T. Haldor, "Geometric correction factors in four point resistivity measurement," Bulletin no. 472-73, http://www.four-point-probes.com/haldor.html.

[26] H. Kawaoka, T. Kusunose, Y. H. Choa, and K. Niihara, "Precise property control in silicon nitride ceramic by α/β phase radio control," *Journal of Ceramic Processing Research*, vol. 2, no. 2, pp. 51–53, 2001.

[27] L. Gao, J. Li, T. Kusunose, and K. Niihara, "Preparation and properties of TiN-Si_3N_4 composites," *Journal of the European Ceramic Society*, vol. 24, no. 2, pp. 381–386, 2004.

[28] C. Y. Tian and N. Liu, "Effect of nano-TiN particles on microstructure and mechanical properties of Si_3N_4-based nanoceramics," *Advances in Applied Ceramics*, vol. 110, no. 4, pp. 205–210, 2011.

[29] W. König, D. F. Dauw, G. Levy, and U. Panten, "EDM-future steps towards the machining of ceramics," *CIRP Annals—Manufacturing Technology*, vol. 37, no. 2, pp. 623–631, 1988.

[30] I. Puertas-Arbizu and C. J. Luis-Pérez, "Revisión de las aplicaciones de la electroerosión por penetración al mecanizado de cerámicas conductoras," *Revista de Metalurgia*, vol. 38, no. 5, pp. 358–372, 2002.

[31] J. S. Thorp and R. I. Sharif, "Dielectric properties of some hot-pressed nitrogen ceramics," *Journal of Materials Science*, vol. 12, no. 11, pp. 2274–2280, 1977.

[32] R. D. Gould and S. A. Awan, "Dielectric properties of RF-sputtered silicon nitride thin films with gold electrodes," *Thin Solid Films*, vol. 433, no. 1-2, pp. 309–314, 2003.

[33] Y. Zhou, H. Hyuga, D. Kusano, Y.-I. Yoshizawa, T. Ohji, and K. Hirao, "Development of high-thermal-conductivity silicon nitride ceramics," *Journal of Asian Ceramic Societies*, vol. 3, no. 3, pp. 221–229, 2015.

[34] F. F. Lange, "Relation between strength, fracture energy, and microstructure of hot-pressed Si_3N_4," *Journal of the American Ceramic Society*, vol. 56, no. 10, pp. 518–522, 1973.

[35] E. Tani, S. Umebayashi, K. Kishi, K. Kobayashi, and M. Nishijima, "Gas-pressure sintering of Si_3N_4 with concurrent addition of Al_2O_3 and 5 wt % rare earth oxide: high fracture toughness Si_3N_4 with fiber-like structure," *American Ceramic Society Bulletin*, vol. 65, no. 9, pp. 1311–1315, 1986.